COBEM 2023 27TH INTERNATIONAL CONGRESS OF MECHANICAL ENGENEERING

ABCM Brazilian Society of Mechanical Sciences and Engineering
27th ABCM International Congress of Mechanical Engineering
December 04-08, 2023, Florianópolis-SC, Brazil

COB-2023-0920
THREE-DIMENSIONAL NAVIER-STOKES SIMULATIONS OF DISPLACEMENT FLOWS BETWEEN MISCIBLE FLUIDS WITH NONMONOTONIC VISCOSITY PROFILES

Bruno Jorge Macedo dos Santos
Rafael Menezes de Oliveira
Dept. Mechanical Eng., Pontifical Catholic University of Rio de Janeiro, PUC-Rio, Rio de Janeiro, RJ, Brazil
rmo@puc-rio.br
brunojorge@aluno.puc-rio.br

Abstract. *Displacements in Hele-Shaw cells, popular as models for corresponding porous media flows, have revealed a wealth of information about viscously and gravitationally driven instabilities. In particular, they have provided fundamental insight into the viscous fingering phenomenon and associated issues of pattern formation. The viscous fingering instabilities are undesirable in many applications as they result in early breakthroughs and reduce the efficiency of the displacement process. It turns out that efficiency can be improved by controlling the mixing length and growth rate of the fingered zone. The present work performs Direct Numerical Simulations by solving the three-dimensional Navier-Stokes equations with variable viscosity to describe displacements in Hele-Shaw cells between miscible fluids with a nonmonotonic viscosity correlation. These correlations are expected to develop reduced mixing lengths when compared to the standard exponential correlation. We investigate shear displacement flows across the gap and reproduce the linear stability results based on the 3D Stokes equations, setting the ground to extend the analysis into the nonlinear fingering regime to carefully capture morphological details of the interfacial structures and calculate displacement efficiencies.*

Keywords: *Three-dimensional Navier-Stokes equations, Hele–Shaw flow, Miscible displacement, Nonmonotonic viscosity profile*

1. INTRODUCTION

Displacements of a viscous fluid by a less viscous one in a Hele-Shaw cell, a confined system between two flat, parallel plates, lead to the formation of Saffman-Taylor instabilities, i.e., ramified structures in the form of viscous fingerings (Hill, 1952; Saffman and Taylor, 1958; Homsy, 1987). This phenomenon has applications in advanced oil recovery and in Carbon Capture, Usage and Storage (CCUS) when carbon dioxide is the injected fluid in the oil reservoir (Li *et al.*, 2023; Chowdhury *et al.*, 2022). Interestingly, thermodynamic conditions of the reservoir may make the carbon dioxide appear in a supercritical state, so displacement processes are influenced by miscibility. In addition, these type of two-phase flows have been of interest to geologists, engineers and scientists for decades.

Despite the progress made on renewable energy, oil and gas remains the world's primary energy source. Meanwhile, large amounts of oil deposits remain unrecovered after application of primary oil recovery methods. Chemical enhanced oil recovery (cEOR) and Water-Alternating-Gas (WAG) have been adjudged as an efficient oil recovery techniques and help produce residual oil trapped in the reservoir. These methods rely on the injection of alternating injected fluids to boost oil recovery (Gbadamosi *et al.*, 2019; Manickam and Homsy, 1994), and lead to displacements in a three-phase system, where the growth of viscous fingers can be reduced by the injection of more than one fluid.

The injected less viscous fluid has higher mobility and penetrates the oil forming branches of viscous fingers, which compromise the displacement efficiency. The description of this phenomenon in multiphase flows between miscible fluids are dominated by diffusion at the interface, by the difference in the viscosity and density of the fluids involved, and by the imposed injection rate (Pinilla *et al.*, 2021). Modelling of multiphase flows are commonly done employing a one-fluid formulation in which the momentum equations is coupled with an advection-diffusion equations for a concentration field that tracks each phase and the miscible interface between them. It turns out that the mixture between different pairs of fluids may render distinct viscosity-concentration correlations, and nonmonotonic functions makes the fluid mixture produce larger viscosity values at the interface between injected and displaced fluids. So, results of these displacement flows can help understand displacements of three-phase systems. In addition, the nonmonotonic profiles are expected to deliver reduced mixing lengths when compared to a monotonically increasing function that relates less and more viscous fluids.

Oliveira and Meiburg (2011, 2013); John *et al.* (2013); Heussler *et al.* (2014); Oliveira and Meiburg (2017) have conducted three-dimensional Navier–Stokes simulations of viscously unstable, miscible Hele-Shaw displacements for the monotonically increasing correlations. Quasisteady fingers are observed whose tip velocity increases with the Péclet

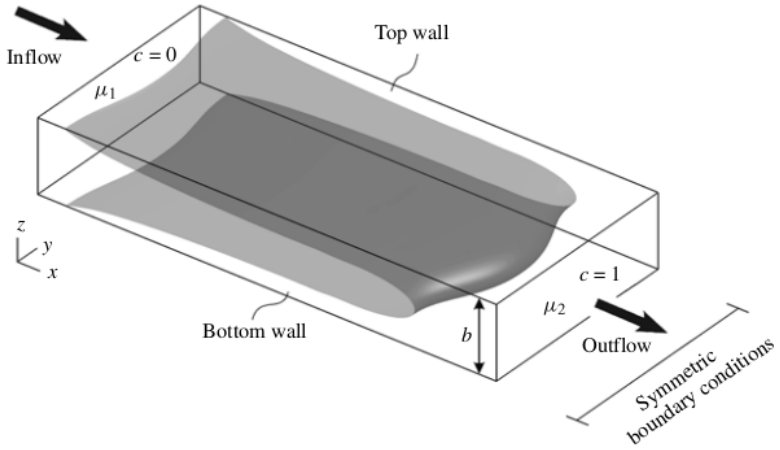

Figure 1. Schematic figure from Oliveira and Meiburg (2011). It shows a shear displacement profile at the xz-plane and the initial growth of a viscous finger in the xy-plane. A uniform developed injection rate is prescribe to drive the displacement process. The injected (displaced) fluid has viscosity μ_1 and $c = 0$ (μ_2 and $c = 1$).

number and the unfavourable viscosity ratio. The simulations reveal the formation of a three-dimensional phenomenon in which the streamwise vorticity across the gap gives rise to an internal splitting that promotes mixture between injected and displaced fluids. In the current work, we begin to expand these results by addressing nonmonotonic viscosity-concentration functions. The momentum equations are coupled to a convection-diffusion equation for the concentration field and the flow is incompressible. We analyze shear displacement patterns across the Hele-Shaw gap and reproduce linear stability results based on the Stokes equations, setting the ground for a three-dimensional nonlinear analysis that captures details of the interfacial dynamics and growth of viscous fingering structures.

2. PHYSICAL PROBLEM

We investigate the displacement between two miscible fluids of different viscosities that are neutrally buoyant and confined in a Hele-Shaw cell, an apparatus given by two parallel horizontal plates separated by a gap b as shown in Figure 1. Considering incompressible flow, the three-dimensional Navier-Stokes equations with variable viscosity is coupled to a convection-diffusion equation for the scalar field, c. This variable denotes the relative concentration of the displaced fluid, so the injected fluid with viscosity μ_1 has $c = 0$, while the displaced fluid has viscosity μ_2 and $c = 1$. Intermediate viscosity values $0 < c < 1$ can be taken as a measure of the diffusive interface.

Dimensionless governing equations are obtained after defining the following characteristic scales: the gap b for length scale, the viscosity of the injected fluid μ_1, and the average velocity of the developed inflow profile U. With these quantities we also define the characteristic time as b/U, and a pressure scale, $\mu_1 U/b$. Thus, the governing equations in terms of non-dimensional variables read

$$\frac{\partial u_k}{\partial x_k} = 0 \tag{1}$$

$$\frac{\partial u_i}{\partial t} + u_k \frac{\partial u_i}{\partial x_k} = \frac{1}{Re}\left\{\frac{\partial}{\partial x_k}\left[\mu(c)\left(\frac{\partial u_i}{\partial x_k} + \frac{\partial u_k}{\partial x_i}\right)\right] - \frac{\partial p}{\partial x_i}\right\} \tag{2}$$

$$\frac{\partial c}{\partial t} + u_k \frac{\partial c}{\partial x_k} = \frac{1}{Pe}\frac{\partial}{\partial x_k}\frac{\partial c}{\partial x_k} \tag{3}$$

Index notation is employed for the above set of equations, which represent the conservation of mass, momentum and species, respectively, with $u_i = (u, v, w)$ indicating the flow velocity; p denotes pressure and t is time. A traditional Cartesian coordinate system $x_k = (x, y, z)$ is used, with x denoting the streamwise direction, while y and z indicate the spanwise and cross-gap directions, respectively.

The numerical algorithm employed uses a hybrid scheme which combines Adams-Bashforth, third order Runge-Kutta and Crank-Nicolson methods for time discretization. We also employ a staggered grid with central differences for the diffusive terms and a fifth-order weighted essentially non-oscillatory upwind scheme for the nonlinear terms. The pressure field is calculated by the projection method and solved by a Poisson equation through direct cosine transform. The code is parallelized with Message Passing Interface. Further discretization details can be found in Oliveira and Meiburg (2011); John *et al.* (2013); Heussler *et al.* (2014).

Notice that we apply a one-fluid formulation and solve the Navier-Stokes equations with the variable viscosity given as a function of the concentrations field. It is represented by a nonmonotonic function, which makes an analogy with a

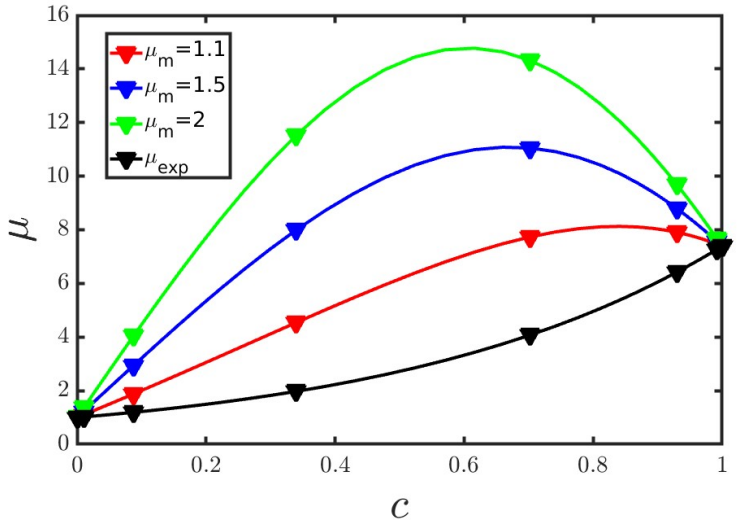

Figure 2. Nonmonotonic viscosity profiles for $\Lambda = 0$ in colors and the exponential viscosity-concentration correlation in black, for comparison.

three-fluid system. As a consequence, the viscosity function denotes the viscosity of the injected and displaced fluids, in addition to the diffuse mixing region that describes the interface. Figure 2 shows a graph that correlates the viscosity in the mixing zone with the concentration field, $0 < c < 1$. The zero concentration, $c = 0$, locates the zone where the injected fluid is found, while $c = 1$ identifies the displaced fluid. For comparison purposes, the black curve shows the monotonically increasing exponential change in viscosity that are typically employed by several authors, including Tan and Homsy (1988); Yortsos and Zeibek (1988); Goyal and Meiburg (2005); Islam and Azaiez (2007); Oliveira and Meiburg (2011); Chen and Meiburg (2017); Cowell *et al.* (2020). The remaining curves represent the non-monotonic viscosity profile Manickam and Homsy (1994); Schafroth (2006); Schafroth *et al.* (2007).

The main dimensionless parameters that governs the dynamics are given by the log-viscosity ratio $M = ln(\mu_2/\mu_1)$, the Reynolds number $Re = \rho Ub/\mu_1$, and the Péclet number $Pe = Ub/D$. The nonmonotonic viscosity profiles have two additional governing parameters. They are the maximum viscosity, μ_m, and

$$\Lambda = \frac{d\mu/dc|_{c=0} + d\mu/dc|_{c=1}}{\mu_2/\mu_1 + 1}. \tag{4}$$

This latter variable depends on the magnitudes of the viscosity gradient at the end points and helps dictate where the maximum in viscosity is located. $\Lambda < 0$ indicates that the slope of the viscosity profile at $c = 1$ is steeper than at $c = 0$, while $\Lambda > 0$ denotes the reverse scenario.

The simulations to be described below will address the low-Reynolds-number regime, and consequently we will employ $Re = 1$ throughout. This is an important initial value which is low enough to permit reproduction of linear growth rates obtained by the three-dimensional Stokes equations conducted by Schafroth *et al.* (2007). More details on the next section.

3. RESULTS

We begin our analysis by advancing the two-dimensional shear displacement profile within the Hele-Shaw cell keeping a uniform front across the spanwise y direction. This situation can be assessed qualitatively from the schematic Fig. 1 by looking at the xz-plane and neglecting fingering growth in the xy-plane. Although this displacement process is physically unstable due to the injection of a less viscous fluid, the development of a viscous finger can only grow in the three-dimensional numerical simulation if a perturbation is introduced as a trigger. As a result, by keeping a uniform spanwise front, we can investigate details of the shear displacement flow. This will be done in the discussion of figures 3, 4 and 5.

Figure 3 shows concentration contours in colors which identify both fluids and their interface, while the black curves display streamlines in a reference frame moving with the tip position located at the $z = 0$ plane. The higher mobility of the injected less viscous fluid makes the blue contours penetrate the yellow one leaving a thin film near the walls. The red arrows point the direction of flow. Notice that recirculation in the form of spanwise vortices are observed inside the displacement front. They drive the formation of the thin film.

Direct Numerical Simulations require that all length scales of the flow are captured. For the current problem, Figure 3 indicates that the location near the tip is where high concentration and velocity gradients are found. So, we track the thickness of the displacement front, $d = x(c = 0.9) - x(c = 0.1)$, and its velocity, and conduct convergence tests of the

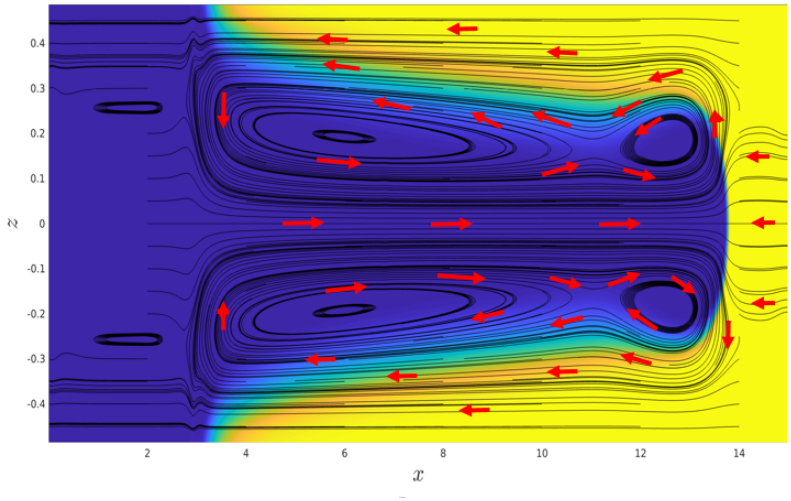

Figure 3. Miscible interface and streamlines of the shear displacement front for $M = 3$, $Pe = 1000$, $Re = 1$, $\Lambda = 0$ and $\mu_m = 1.1$.

numerical algorithm.

Figures 4 exemplifies this behavior by showing the time evolution of the front thickness for $(M, Re, Pe, \mu_m, \Lambda) = (3, 1, 2000, 1.1, 0)$. The injected fluid compresses the interface and the front thickness reaches a minimum quasisteady value. However, according to Schafroth *et al.* (2007), when diffusion outweighs convection a steep front thickness cannot be sustained. As a consequence, the front thickness increases for later times. Figures 4 also provides a convergence test by considering three different spatial resolutions. The red curve indicates 80 points per unit length, the blue curve indicates 100 points per unit length, and the green curve has 120 points per unit length. Notice that comparison between the curves suggests that 100 points per unit length is a good resolution, having a small error in comparison to the green curve. This will be the resolution used in the remaining simulations.

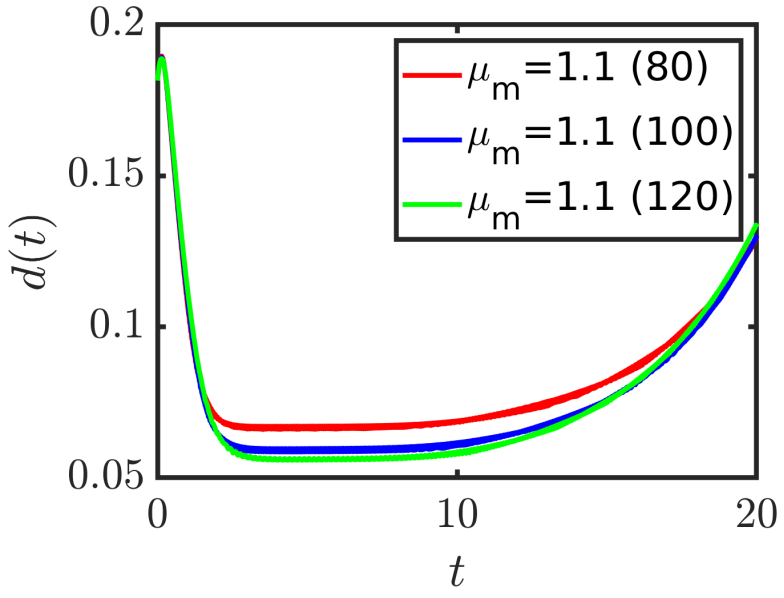

Figure 4. Evolution of the front thickness for the same parameters used in Fig. 3. Different mesh resolutions are displaced in the legend and represent the number of grid points per unit length. These results also serve as a convergence test.

Figure 5 shows the time evolution of the tip velocity, defined as the streamwise velocity u for the $c = 0.5$ concentration contour at $z = 0$ for $(M, Re, Pe, \Lambda) = (3, 1, 2000, 0)$. Different curves display results for different values of the maximum viscosity, $\mu_m = 1.1$ for the blue curve, and $\mu_m = 1.5$ for the red one. It shows that the displacement front for neutrally buoyant flows, $F = 0$, achieve a steadily advancing front. Moreover, by increasing the maximum viscosity from $\mu_m = 1.1$ to $\mu_m = 1.5$ while keeping fixed the end-point viscosities, we observe a subtle decrease in the quasisteady velocity value.

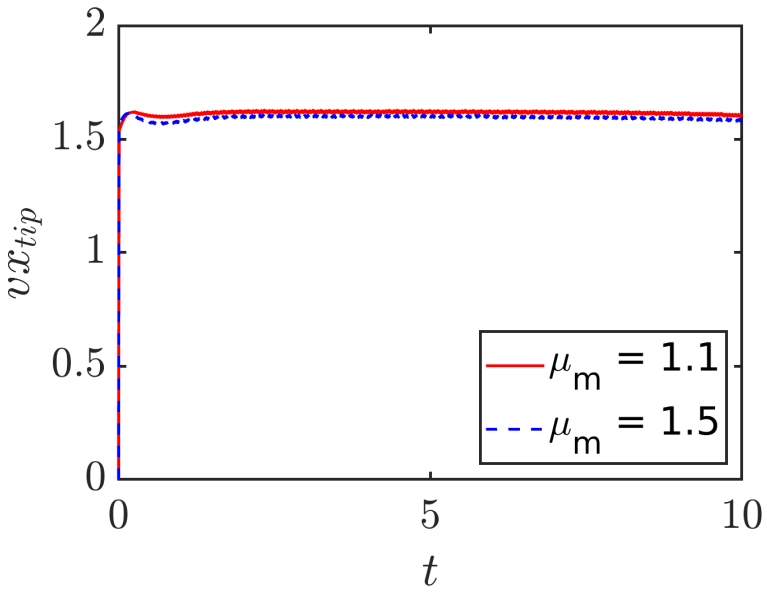

Figure 5. Evolution of the tip velocity for two different values of the maximum viscosity, μ_m fro the same remaining parameters as in Figs. 3 and 4.

3.1 LINEAR GROWTH RATES

To initiate the three-dimensional analysis, we impose a sine disturbance in the flow at time $t = 4$ when the interface front has reached a quasisteady configuration with fixed front thickness and uniform tip velocity. This perturbation is expected to trigger the growth of a viscous finger. We choose the wavelength of maximum growth as predicted by the linear stability analysis of Schafroth *et al.* (2007) based on the three-dimensional Stokes equations and set the spanwise domain to the size of a single wavelength. The wave amplitude of the disturbance is set to $\xi(t = 4) = 0.0001$, which is small enough so the finger grows linearly before advancing to nonlinear stages of the dynamics.

Figure 6 plots the time evolution of the wave amplitude growth, $\xi(t)$, for $Pe = 2000$, $Re = 1$, $\mu_m = 1.1$, $\Lambda = 0$, and two different values of the ratio between the end-point viscosities, $M = 2$ and $M = 3$. The linear plots in log scale indicates exponential growth, confirming the expectation of fingering growth in the linear regime when a wavy disturbance of small amplitude is imposed. The growth rate is given by the inclination of these curves, and their values are close to the ones reported by Schafroth *et al.* (2007). This also indicates that $Re = 1$ is small enough to reproduce results from an analysis based on the Stokes equations. In addition, these results help corroborate the accuracy of the numerical algorithm in the third dimension.

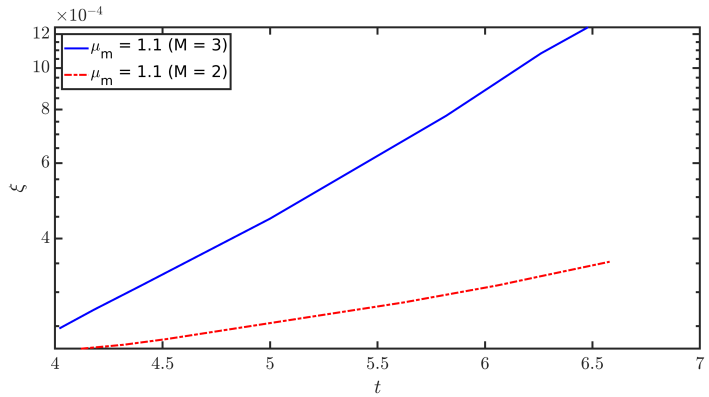

Figure 6. Evolution of the small wave amplitude describing the onset of fingering growth for $(M, Re, Pe, \mu_m, \Lambda) = (3, 1, 2000, 1.1, 0)$ and $(M, Re, Pe, \mu_m, \Lambda) = (2, 1, 2000, 1.1, 0)$. A linear plot in log scale indicates exponential growth. The indication of this curve is used to reproduce growth rate results from the linear stability analysis based on the 3D Stokes equations of Schafroth *et al.* (2007).

4. CONCLUSIONS

We are investigating the growth os viscous fingers in a Hele-Shaw cell by solving the three-dimensional variable viscosity Navier-Stokes equations coupled to a convection-diffusion equation for a scalar field that tracks the concentration of the displaced fluid. The variable viscosity function is correlated to the concentration field by a nonmonotonic function, so depending on the proportion of the mixture, the resulting fluid may be more viscous than either the injected or displayed fluids. This behavior is expected to reduce mixing lengths which may lead to improved displacement efficiencies. We also highlight that these type of multiphase flows have applications in chemical Enhanced Oil Recovery (cEOR) and Carbon Capture, Usage and Storage (CCUS).

The 3D description captures details of the dynamics across the gap and shear displacement fronts have been described. For the parameters investigated, these fronts achieve a quasisteady value with a nearly constant front thickness that advances with a fixed velocity value. After adding a wavy perturbation of small amplitude, we have observed the onset of fingering growth and reproduced growth rate results of a linear stability analysis based on the 3D Stokes equations. Future works shall investigate fingering growth into the nonlinear dynamics and obtain a complete description of the growth of a single miscible viscous finger for nonmonotonic correlations. We also plan to investigate wider spanwise domains to describe details of the dynamics including multiple fingers and competition between them. This should allow us to address some important questions. For example, discrepancies in fingering growth have been observed between two-dimensional gap-averaged descriptions such as Darcy's law and three-dimensional analyses, cf. Oliveira and Meiburg (2017). What are the parameter ranges in which the 2D modeling are valid? Can we modify gap-average laws to incorporate phenomena only captured by a three-dimensional description? The inner-splitting mechanism (Oliveira and Meiburg, 2011) is one of these features and it has been observed for pair of fluids that satisfy a exponential viscosity-concentration correlation. Does this phenomena also appear for the nonmonotonic correlation? The current work sets the ground for addressing some of these questions.

5. ACKNOWLEDGEMENTS

The authors thank the Brazilian Government agencies CAPES, CNPq and ANP for the continuous support during the development of this research.

6. REFERENCES

Chen, C.Y. and Meiburg, E., 2017. "Miscible displacements in capillary tubes. part 2. numerical simulations." *Phys. Rev. Lett.*, Vol. 118(12), p. 124502.

Chowdhury, S., Rakesh, M., Medhi, S., Trivedi, J. and Sangwai, J., 2022. "Pore-scale flow simulation of supercritical co_2 and oil flow for simultaneous co_2 geo-sequestration and enhanced oil recovery". *Environmental Science and Pollution Research*, Vol. 29, pp. 76003–76025.

Cowell, S., Kent, J. and Trevelyan, P.M.J., 2020. "Rayleigh-taylor instabilities in miscible fluids with initially piecewise linear density profiles". *Journal of Engineering Mathematics*, Vol. 121, pp. 57–83.

Gbadamosi, A.O., Junin, R., Manan, M.A., Agil, A. and Yusuff, A.S., 2019. "An overview of chemical enhanced oil recovery: recent advances and prospects". *International Nano Letters*, Vol. 9, pp. 171–202.

Goyal, N. and Meiburg, E., 2005. "Miscible displacements in hele-shaw cells : two-dimensional base states and their linear stability". *J. Fluid Mech.*, Vol. 558, pp. 329–355.

Heussler, F.H.C., Oliveira, R.M., John, M.O. and Meiburg, E., 2014. "Three-dimensional navier–stokes simulations of buoyant, vertical miscible hele-shaw displacements". *J. Fluid Mech.*, Vol. 752, No. 157-183.

Hill, S., 1952. "Channeling in packed columns". *Chem. Eng. Sci.*, Vol. 1, No. 6, pp. 247 – 253.

Homsy, G.M., 1987. "Viscous fingering in porous media". *Annu. Rev. Fluid Mech.*, Vol. 19, pp. 271–311.

Islam, M.N. and Azaiez, J., 2007. "New viscous fingering mechanisms at high viscosity ratio and péclet number miscible displacements." *J. Porous Media*, Vol. 10(4).

John, M.O., Oliveira, R.M., Heussler, F. and Meiburg, E., 2013. "Variable density and viscosity, miscible displacements in horizontal hele-shaw cells. part 2. nonlinear simulations". *J. Fluid Mech.*, Vol. 721, pp. 295–323.

Li, D., Zhong, Y. and Jiang, X., 2023. "Experimental study of impurity effects on convective mixing in hele-shaw cell with application to co_2 geological sequestration". *Advances in Water Resources*, Vol. 172, p. 104379.

Manickam, O. and Homsy, G.M., 1994. "Simulation of viscous fingering in miscible discplacements with nonmonotomic viscosity profiles". *Physics of Fluids*, Vol. 6, p. 107.

Oliveira, R.M. and Meiburg, E., 2011. "Miscible displacements in hele-shaw cells: three-dimensional navier–stokes simulations". *Journal of Fuid Mechanics*, Vol. 687, pp. 431–460.

Oliveira, R.M. and Meiburg, E., 2013. "Three-dimensional vorticity configurations in miscible hele-shaw displacements". *Proc. IUTAM*, Vol. 7, No. 203-212.

Oliveira, R.M. and Meiburg, E., 2017. "Saffman-taylor instability and the inner splitting mechanism". *Physical Review*

Letters, Vol. 118, p. 124502.

Pinilla, A., Asuaje, M. and Ratkovich, N., 2021. "Experimental and computational advances on the study of viscous fingering: An umbrella review". *Heliyon*, Vol. 7, p. 29.

Saffman, P.G. and Taylor, G.I., 1958. "The penetration of a fluid into a porous medium or Hele-Shaw cell containing a more viscous liquid". *Proc. R. Soc. London. Ser. A*, Vol. 245, No. 1242, pp. 312–329.

Schafroth, D., Goyal, N. and Meiburg, E., 2007. "Miscible displacements in hele–shaw cells: Nonmonotonic viscosity profiles". *European Journal of Mechanics B/Fluids*, Vol. 26, pp. 444–453.

Schafroth, D., 2006. *Influence of non monotonic viscosity profiles on the stability of miscible displacement flows in a Hele-Shaw cell*. Ph.D. thesis, Institute of Fluid Dynamics Department of Mechanical Engineering, ETH, Zurich, Switzerland.

Tan, C.T. and Homsy, G.M., 1988. "Simulation of nonlinear viscous fingering in miscible displacement." *Phys. Fluids*, Vol. 31(6), pp. 1330–1338.

Yortsos, Y.C. and Zeibek, M., 1988. "Dispersion driven instability in miscible displacement in porous media." *Phys. Fluids*, Vol. 31(12).

7. RESPONSIBILITY NOTICE

The authors are solely responsible for the printed material included in this paper.